PAPER • OPEN ACCESS

MXene photocatalysts for microplastics degradation under simulated solar illumination

IOP Publishing J. Phys. Mater. 8 (2025) 045012 https://doi.org/10.1088/2515-7639/ae0d00

Journal of Physics: Materials

OPEN ACCESS

RECEIVED
3 June 2025

REVISED
5 August 2025

ACCEPTED FOR PUBLICATION
29 September 2025

PUBLISHED
14 October 2025

PAPER

MXene photocatalysts for microplastics degradation under simulated solar illumination

Atta Ur Rehman[1], Sin Yi Pang[2], Kang Ding Han[3], Chunyang Dong[4], Yingchuan Zhang[4], Yanling He[5], Christelle A Not[6], Alan Man Ching Ng[7], Jianhua Hao[2], Jasminka Popović[8,*], Zheng Xiao Guo[4,*] and Aleksandra B Djurišić[1,8,*]

[1] Department of Physics, The University of Hong Kong, Pokfulam, Hong Kong Special Administrative Region of China, People's Republic of China
[2] Department of Applied Physics, The Hong Kong Polytechnic University, Hung Hom, Hong Kong Special Administrative Region of China, People's Republic of China
[3] Department of Chemistry, National University of Singapore, 21 Lower Kent Ridge Rd, Singapore 119077, Singapore
[4] Department of Chemistry, The University of Hong Kong, Pokfulam, Hong Kong Special Administrative Region of China, People's Republic of China
[5] Material characterization and preparation facility, The Hong Kong University of Science and Technology (Guangzhou), No.1 Duxue Road, Dongchong Town, Nansha District, 511458 Guangzhou, Guangdong Province, People's Republic of China
[6] Department of Earth and Planetary Science, The University of Hong Kong, Pokfulam, Hong Kong Special Administrative Region of China, People's Republic of China
[7] Department of Physics & Core Research Facilities, Southern University of Science and Technology, Shenzhen 518055, People's Republic of China
[8] Division of Materials Physics, Ruđer Bošković Institute, Bijenička 54, 10000 Zagreb, Croatia
[*] Authors to whom any correspondence should be addressed.

E-mail: Jasminka.Popovic@irb.hr, zxguo@hku.hk and dalek@hku.hk

Keywords: MXene, photocatalysis, microplastics

Supplementary material for this article is available online

Abstract

Microplastics (MPs) pollution is a widespread and growing problem. Consequently, there is significant interest in photocatalytic degradation and/or conversion of MPs, especially in the case of polyolefins, which are the dominant type of plastic waste and which are difficult to degrade due to their stable C–C backbones. Thus, complete mineralization of polyolefins, as well as their conversion to fuel or other chemicals, is highly challenging and requires the development of novel photocatalyst materials. Here, we investigate an MXene photocatalyst for photocatalytic conversion of polyethylene (PE) plastics in aqueous solutions with and without NaOH. In the absence of NaOH, Ti_2CT_x MXene results in complete mineralization of pristine PE as well as environmental PE MPs, with CO_2 as the dominant reaction product. In contrast, with the addition of 5 M NaOH, hydrogen becomes the dominant product with a high activity exceeding 500 μmol g_{cat}^{-1}.

1. Introduction

Microplastics (MPs), defined as plastic fragments smaller than 5 mm and larger than 1 μm, are ubiquitous and persistent pollutants, which have been attracting increasing attention due to their potential adverse environmental impact [1–6]. MPs can be intentionally produced MPs (primary MPs) or created by fragmentation of larger plastics [1]. As the amount of plastic waste continues to rise with ocean plastics waste expected to reach 250 Mt in 2025 and exceed the weight of fish by 2050 [1, 6], MPs pollution is also rising. MPs have already infiltrated the food chain, resulting in concerns for their effect on human health due to their demonstrated presence in human bodies [4, 5]. In addition, MPs have wide-ranging effects on the environment and ecosystems, as their accumulation leads to alterations in carbon-dependent soil functions, which impacts plant growth and heavy metal availability [7, 8]. While the ingestion of MPs typically does not lead to fatalities due to acute toxicity, the long-term exposure results in chronic toxicity for a variety of different organisms [1]. In addition, various additives and heavy metal complexes present in commercial

plastics can also result in significant toxicity as they leach out of MPs in the environment [1]. Due to the rapidly increasing MPs contamination in the environment and their resistance to degradation, the development of efficient methods to address MPs pollution is imperative [1].

It is also critically important that the developed methods for tackling MPs pollution involve permanent transformation of MPs. This is particularly challenging for polyolefin MPs, due to their remarkable stability owing to their C–C backbone [1]. While physical separation methods used in waste water treatment plants (WWTPs) can efficiently remove MPs, the reuse of WWTP sludge in agriculture results in the return of 44–300 kt of MPs into the environment in North America alone [1]. The MPs deposited on farmland can be absorbed by plants or re-enter waterways via runoff and soil erosion [1]. Unlike physical separation methods, chemical degradation (photocatalysis, catalysis, advanced oxidation processes) and biodegradation can achieve permanent removal of MPs [1]. Among these methods, photocatalysis is of particular interest since it is performed under mild conditions (no elevated temperature or pressure needed) [3], and it can be used to achieve photocatalytic degradation (complete mineralization of MPs into nontoxic products such as CO_2 and H_2O), as well as photocatalytic conversion/upcycling to produce fuels and/or useful chemicals [1]. While photocatalytic degradation contributes to CO_2 emissions, as CO_2 is most commonly obtained as a major product of the degradation [6], it can eliminate toxic pollutant MPs and it is suitable for plastics with different compositions and containing different additives and/or contaminants. Consequently, this process is uniquely suitable for degradation of mixed MP samples collected from the environment, and there is considerable interest in achieving complete removal of environmental MPs, in addition to interest in upcycling. As a result, a number of different photocatalyst materials for degradation and/or upcycling of waste plastics have been investigated to date [9–35]. However, in a significant majority of those reports, degradation efficiencies are commonly relatively low, with very few exceptions achieving degradation efficiencies exceeding 90% [2, 3, 12, 13, 22, 23]. Thus, there is a need for further development of photocatalysts capable of complete mineralization of MPs.

In addition, due to the increasing interest in the generation of fuels and useful chemicals from MPs [31–33], it is desirable to develop photocatalysts which could produce useful chemicals instead of CO_2, especially from polyolefin plastics, such as polyethylene (PE) and polypropylene (PP) which represent over 50% of all the plastics produced [33]. Reports on photocatalytic upcycling of various plastics, such as polylactic acid (PLA), PE terephthalate (PET), polyurethane (PUR), PE, PP, etc, are summarized in table S1. From table S1, it can be observed that the most commonly considered plastics for upcycling are those containing C–O backbones such as PLA and PET, while the reports on hydrogen production from PE or PP degradation have been scarce [24–30]. Thus, we investigated the degradation of PE as a model material under different conditions in an attempt to adjust the reaction products. Since PE cannot be depolymerized into short-chain monomers by alkaline pre-treatments, unlike hetero-backbone plastics such as PET, PUR, etc [31–34], various pretreatment processes and degradation solutions have been reported for PE. In some cases, no pre-treatments were specified [24, 26], while in others nitric acid at high temperature [25, 27] or alkaline pre-treatments [29, 30] were used. A very high H_2 production (of the order of $\sim$17 mmol h^{-1} $g_{cat}{}^{-1}$) was reported for the reaction in 5 M NaOH PE solution under illumination by a 400 W Xe lamp [29], here we investigated the effects of NaOH on the degradation of PE in aqueous solutions.

As carbon-based materials are promising photocatalysts for photo-reforming of plastics [35], we investigated the use of MXene photocatalyst Ti_2CT_x MXene materials produced by optimized HF-free synthesis process have excellent –O/–OH surface coverage and have been shown to exhibit high hydrogen evolution rates as electrocatalysts [36]. In general, MXenes have been shown to be highly promising for various photocatalytic applications, such as water splitting, CO_2 reduction, and pollutant degradation [37–40], including H_2 evolution from photocatalytic degradation of PET using MXene/$Zn_xCd_{1-x}S$ [40], but they have not been explored for photocatalytic conversion of polyolefins. We find that Ti_2CT_x MXene exhibited excellent photocatalytic activity for degradation of PE. In addition, the degradation in alkaline solutions has resulted in a significant change in the composition of evolved gases as a result of photocatalytic PE degradation. Compared to other reports on the production of H_2 from PE degradation, the obtained activity is not as high as that for high activity material combinations [24, 25, 27, 29], although it is significantly higher compared to some literature reports [30]. However, unlike previous reports, there is no use of noble metals such as Pt [25], or toxic metals such as Co and Cd [24, 27, 29]. Furthermore, harsh pretreatment conditions, such as HNO_3 pretreatment at 180 °C [25, 27], are not used. Thus, while the time needed for complete degradation under neutral conditions is comparable to the best reported results (Nb_2O_5 photocatalyst) [12], hydrogen evolution under alkaline conditions is not as high as in the case of metal-semiconductor [24, 25] or semiconductor heterojunction [27, 29] photocatalysts.

The most interesting aspect of our work is the shift in the composition of the evolved gases from CO_2 dominated (0 M) over CH_4 dominated (2 M) to H_2 dominated (5 M). This shift is specific to MXene and it does not occur for other photocatalysts capable of PE degradation, such as Nb_2O_5. Thus, we expect that this

investigation can facilitate further development of novel photocatalysts based on MXene or metal carbide materials more generally, which would exhibit better yield and stability compared to pure MXene while retaining the ability to tune the composition of evolved gases while changing pH.

2. Results and discussion

Figure 1 shows XRD patterns, crystal structures and SEM images for the Ti_2AlC MAX 211 phase and Ti_2CT_x MXene phase, receptively. The MXene phase was obtained by HF-free synthesis from the MAX 211 precursor using the previously reported procedure [36]. The MAX Ti_2AlC phase crystallizes in a $P6_3/mmc$ space group with unit-cell parameters $a = 3.062(1)$ Å and $c = 13.668$ Å. The structure can be considered as a laminated composite that consists of edge-sharing Ti_6C octahedral layers along the c-axis with Al layers inserted between every two carbide sheets. Although the etching process removes the Al layers, and thus destroys the parent's long-range hexagonal symmetry, it does not eliminate the layered nature of the MXene. Instead, a stack of parallel 2D Ti–C–Ti sheets remain and therefore a short-range order along the c-axis is observed from the 00 l reflections. As a result of functionalization, the interlayer periodicity of stacked Ti_2C–T_x sheets in MXene increased to $d = 13.5$ Å, which is significantly larger than that of MAX ($d = 6.86$ Å). An SEM image of the MXene phase before delamination is given in figure S1.

To evaluate the photocatalytic activity of MXene, we performed photocatalytic degradation of pure and environmental PE plastics, as shown in figure 2. The morphology of pure PE particles is shown in figure 3(a), while the corresponding size distribution is shown in figure S2, indicating an average PE size of 7.7 μm. The experiments performed in water solutions resulted in a 100% mass loss of pristine PE, as illustrated in figure 2(a). This is consistent with the observed disappearance of plastic particles in the SEM images (figure 3(b)), where the shape and contrast of particles is consistent with MXene, which is more conductive compared to plastics and contains sharp edges of thin layers. We can also observe the presence of Ti in the EDX spectra of detectable particles in figure 3(b), in clear contrast with EDX spectra of PE, as shown in figure S3. In addition, from EDX mapping of the samples after illumination, shown in figure S4, we can observe not only the clear presence of Ti in the micron-sized layered aggregates but also a significant increase in the Ti:C ratio due to decomposition of plastics which contains only carbon, while MXene samples contain both Ti and C. The observation of 100% mass loss of PE is also consistent with the reduction in particle size over time determined by dynamic light scattering, as shown in figure S5. The observed decrease in particle size is similar to observations of photocatalytic degradation of polystyrene nanoparticles [22]. Figure S6 shows the FTIR spectra of the PE before and after 24 h of illumination. Before illumination, only characteristic PE-specific peaks, corresponding to C–C and C–H vibrations, are observed [23, 41]. After illumination, we observe a significant decrease in peak intensity, as evidenced from decreased signal to noise ratio, as well as the appearance of a number of additional weak peaks, which could possibly be attributed to different C=O and C=C stretching (1500–2500 cm^{-1}), as well as C–O stretching (1000–1200 cm^{-1}) [41]. In addition to pristine PE, we have also investigated the photocatalytic degradation of environmental plastics. Environmental plastic samples were collected in Hong Kong following the previously reported procedures [23, 42, 43]. A selected piece of plastic (inset of figure S7) was identified as PE from the FTIR spectra, shown in figure S7. In addition to the characteristic PE peaks, in the environmental PE sample we can observe peaks corresponding to OH vibrations (3000–3500 cm^{-1}), as well as C=O vibrations (1500–1800 cm^{-1}) [41], as expected for a weathered plastic sample [23]. We observe a similar degradation rate for pristine (figure 2(a)) and environmental PE (figure 2(b)), with ~50% degraded in 24 h. The determined mass loss for environmental PE could not reach 100% due to the limitation of balance used for mass measurements (a similar limitation is observed in the same balance for pristine PE, as shown in figure S6). No observable plastics could be seen by the naked eye in the environmental sample after 48 h, and from comparison of PE degradation with different balances used for mass loss measurement, we can assume that complete degradation occurred in this case as well. To further confirm the effectiveness of Ti_2CT_x MXene for degradation of environmental MPs, an additional experiment has been conducted, using a sample consisting of mixed small MPs and a balance with a hanging mass pan. From the results shown in figure 4, we can observe that complete degradation is achieved. Furthermore, from the FTIR spectrum of this sample and the observed peaks in the region 2800–3000 cm^{-1}, we can conclude that the sample contained PP MPs as additional peaks compared to PE, in agreement with the characteristic peaks of PP [10].

To investigate the species produced during the degradation, experiments were repeated in a closed photocatalytic reactor, and the gases produced were analyzed by gas chromatography (GC). The obtained results are shown in figures 5 and 6 and summarized in table S2. We can observe that in the absence of NaOH (normal conditions for PE degradation in an open reactor in ambient), the major degradation product is CO_2, with small amounts of CO and CH_4. CO_2 is commonly observed as the main degradation product of photocatalytic degradation of PE [12, 22].

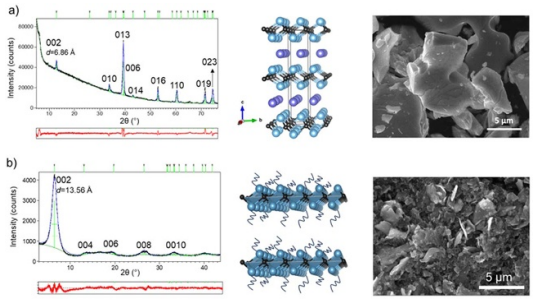

Figure 1. XRD patterns, crystal structures and SEM images for (a) Ti_2AlC MAX 211 phase and (b) Ti_2CT_x MXene phase (after delamination). Experimental x-ray diffraction data are given as black dots, calculated pattern in shown in blue while green vertical marks represent the position of reflections. The difference curve in given below, in red. Ti atoms are shown as blue balls, carbon atoms are given in black while the Al is violet.

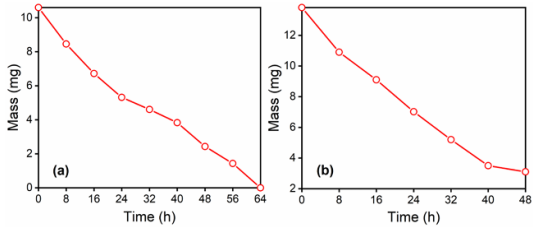

Figure 2. Remaining mass as a function of illumination time for (a) model PE plastics and (b) environmental PE plastics. The experiment was performed at 0 M NaOH.

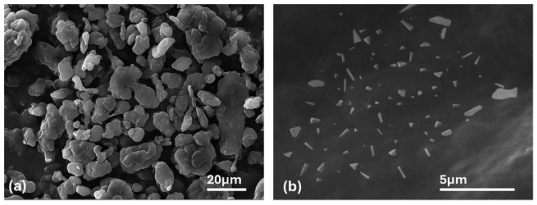

Figure 3. SEM images of (a) model PE MPs (b) PE +MXene after 48 h of illumination (0 M NaOH).

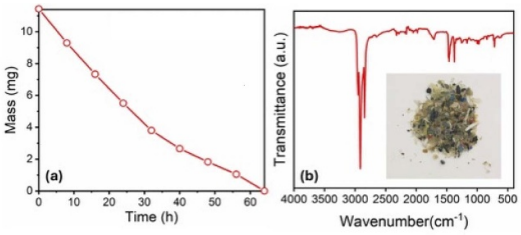

Figure 4. (a) Remaining mass as a function of time of illumination for environmental MP sample (b) FTIR spectrum of the environmental MP sample. Inset shows the photo of the environmental sample. The experiment was performed at 0 M NaOH.

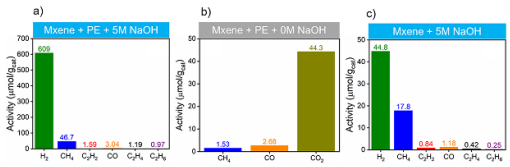

Figure 5. Production of different gases during photocatalytic degradation of PE with MXene photocatalyst for (a) 5 M NaOH (b) 0 M NaOH. (c) Production of different gases during illumination of MXene photocatalyst without PE for 5 M NaOH.

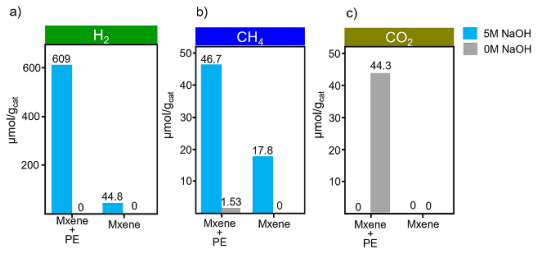

Figure 6. Comparison of different reaction conditions for production of (a) H_2, (b) CH_4, and (c) CO_2.

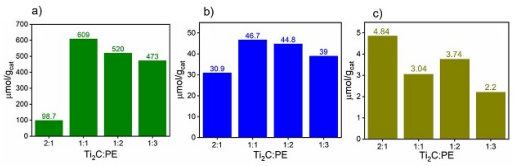

Figure 7. Comparison of different photocatalyst:PE ratios for production of (a) H_2, (b) CH_4, and (c) CO.

From figures 5 and 6 and table S2, we can observe that CO_2 is produced only in the presence of PE, and the production of CO_2 disappears under alkaline conditions. While the use of NaOH is not expected to result in depolymerization of PE, different from PET and PLA, high H_2 production in the literature has been reported for alkaline reaction solutions for different photocatalysts, such as Co_3O_4/g–C_3N_4 and brookite TiO_2 [28, 29], although for other materials, such as CN_x/Ni_2P [30], a significantly lower production rate of the order of 5–6 μmol g_{cat}^{-1} h^{-1} was reported in 1 M KOH solution. In addition to H_2 produced under alkaline conditions, we can also observe the production of CH_4, CO, C_2H_2, C_2H_4 and C_2H_6. The other products are present in significantly lower quantities than H_2, with the amount of CH_4 produced 13 times lower than that of H_2, while for the other gases the product amount is over 200 times lower than that of H_2. From the optimization of the MXene:PE ratio, shown in figure 7, we can observe that the highest amount of hydrogen is produced at a 1:1 ratio, while the lowest amount of CO is obtained at a 1:3 ratio.

If we examine the gases produced for different reaction times, as shown in figure S9, we can see that H_2 production starts to dominate at 24 h. In earlier stages of degradation, CO_2 can be detected, but its concentration decreases with increasing illumination time. It has been reported that CO_2 containing liquid products rather than gaseous CO_2 are obtained by photocatalysis of plastics in alkaline medium [30], so the reduction of CO_2 in gas phase could be because of its dissolution, possibly combined with participation in additional reactions as MXene can work as a photocatalyst for CO_2 reduction [39]. We can also observe that the concentration of NaOH affects the composition of the evolved gases, as shown in figure S10. After 24 h of illumination for 2 M NaOH solution, the dominant product is CH_4, followed by H_2 and CO. To clarify the contributions of the photocatalyst used and alkaline reaction conditions to the evolution of H_2, we have performed an experiment in a 5 M NaOH solution using Nb_2O_5 nanoparticles. Nb_2O_5 is capable of degrading different plastics [12], but no hydrogen evolution is observed, as shown in figure S11, and the overall yield of gas products is small. Thus, we can conclude that the Ti_2CT_x photocatalyst plays an essential role in H_2 evolution from alkaline suspensions of PE, with the MXene capability for both CO_2 reduction and water splitting contributing to the unique composition of evolved gases. Furthermore, while we can see significant production of H_2 from PE + Ti_2CT_x and 5 M NaOH, we can also observe that H_2 is produced in the absence of PE, as shown in figure 5(c), which is not surprising since MXene can be used for photocatalytic H_2 production [37]. In addition, the production of hydrogen, with activity reducing from 7.66 to 1.67 μmol g_{cat}^{-1} h^{-1} from 2 h to 25 h, was previously reported in the absence of plastics for the CN_x/Ni_2P photocatalyst in aqueous KOH, which was attributed to residue from photocatalyst synthesis based on an initially higher rate [30]. Nevertheless, production of hydrogen in the absence of substrate continued for up to 120 h at a rate 0.7 μmol g_{cat}^{-1} h^{-1}, with no significant decrease in the rate observed after 48 h [30]. Here, we observe an average rate of 1.87 μmol g_{cat}^{-1} h^{-1} (determined at 24 h), which is comparable to the previous report [30]. However, we can also observe the production of CH_4 and CO (figure 5(c)), although in significantly lower amounts compared to the MXene:PE case (figure 5(a)). MXene containing photocatalysts is also capable of photocatalytic CO_2 reduction [39], but the most likely source of carbon is Ti_2CT_x itself as the presence of CO_2 in water without PE is expected to be very low. Furthermore, it

is known that MXene can be oxidized in aqueous solutions under UV illumination [37]. Alkaline environments can be oxidizing, negatively affecting the MXene stability due to its susceptibility to oxidation [37, 44]. It has been shown that $Ti_3C_2T_x$ MXene oxidizes to TiO_2 in the presence of oxygen in alkaline solutions [44]. However, no production of H_2 is detected from alkaline solutions of PE with P25 TiO_2, as shown in figure S12. We can observe that the amount of evolved gases with TiO_2 is even lower compared to PE without photocatalyst, which indicates that if any TiO_2 is produced, it does not contribute significantly to photocatalytic PE degradation.

As the changes in both photocatalyst and PE degradation products occur in an alkaline environment, it is necessary to understand these changes. However, the quantification of degradation of PE in alkaline solutions is hampered by difficulties in determining the mass loss. Nevertheless, we observe similar sizes of PE particle aggregates after 24 h of illumination in a closed reactor used for gas product analysis for 0 M and 5 M NaOH, as shown in figure S13. However, detailed examination of the PE degradation in alkaline solutions still remains difficult as it is difficult to dry and isolate smaller particles. To understand the reasons for the difficulties in measuring mass loss in alkaline solutions (higher mass of dried products after degradation), we examined the degradation products in alkaline solutions. We found that the samples do not completely dry for a long time (over 72 h at 100 °C in a vacuum oven), as shown in figure S14, and when dried produce large crystals due to the presence of NaOH and possibly reactions between NaOH and any dissolved CO_2 as bases are known to react with dissolved CO_2 [12, 24]. These reactions could also possibly account for the absence of CO_2 in evolved gases from the PE degradation in alkaline solutions. In contrast, samples could be dried for 2 M NaOH solutions at a lower temperature (70 °C), as shown in figure S15. It should also be noted that the dried samples from alkaline solutions are highly hygroscopic, which imposes additional difficulties in their characterization in high ambient humidity environments (in ambient humidity of ∼65% in our laboratory, any dried samples from 5 M solutions quickly rehydrate from powder/crystals into gel-like material).

Since the alkaline environment is also expected to result in an increase in surface OH group concentration, which is known to have a positive impact on CO_2 reduction [37], FTIR measurements were used to characterize the effect of alkaline solution on Ti_2CT_x MXene. The obtained FTIR spectra for MXene after immersion in 0 M and 5 M NaOH solutions are shown in figure S16. We observe that samples with and without illumination and without exposure to NaOH (0 M samples) exhibit a broad band in the region 3000–3500 cm^{-1} corresponding to OH vibrations [41], and two peaks at ∼1620 cm^{-1} and ∼1400 cm^{-1}. There are multiple possible assignments in this spectral region, but from the absence of characteristic peaks in other spectral regions we can rule out aliphatic C–H vibrations [41]. Consequently, the observed peaks could possibly correspond to C=O, C=C, and C–O vibrations. The lack of change in FTIR spectra after illumination for the 0 M sample is consistent with the lack of evolution of any gases under illumination and indicates that the samples have good photostability without NaOH. However, in the case of the 5 M sample, we observe significant changes in the FTIR spectra, with a significant increase in OH vibrations, and the appearance of multiple new peaks in spectral regions where various C=O, C–O, and C–O–C vibrations are expected to be observed [41]. While FTIR measurements are not quantitative, there is a clear increase in the intensity of these peaks compared to the broad OH vibrations peak. This indicates that NaOH oxidizes the surface of MXene, significantly increasing the number of reactive functional groups at the surface, which is likely responsible for the observed changes in the photocatalytic degradation products for 5 M solutions. From the SEM images of MXene after immersion in 5 M NaOH with and without illumination, figure S17, there was no significant change in the size and morphology of the MXene after illumination. However, both samples (with and without illumination) exhibited different morphology compared to samples before immersion in alkaline solution. After immersion in 5 M NaOH, wire-like morphologies were observed on the surface because the concentrated alkali hydrolyzed part of the MXene nanosheets into nanowires [45].

Figure 8 shows the Rietveld refinement analysis that has been performed on dried products obtained after the reaction with 2 M NaOH after 8 h of illumination, and after drying at 35 °C under vacuum for 10 h. Rietveld refinement revealed thedried product contains, as expected, MXene catalyst but also a small amount of rutile TiO_2 as confirmed from the refined unit-cell parameters of $a = 4.61(2)$ Å and $c = 2.98(1)$ Å in the $P4_2/mnm$ space group. The presence of rutile indicates that the partial oxidation of MXene took place. Depending on the drying conditions, as well as MXene and rutile, the dry product can contain γ-polymorph of sodium carbonate (Na_2CO_3) as confirmed by the refined unit-cell parameters $a = 8.94(1)$ Å, $b = 5.25(2)$ Å, and $c = 6.02(4)$ Å, with a monoclinic angle $\beta \approx 102.2(2)$ °, which is expected to result from the reaction between NaOH and dissolved CO_2 [12, 24]. As no photocatalytic activity for H_2 production is observed in pure TiO_2 samples (P25 consisting of anatase and rutile, figure S12), the production of H_2 in alkaline solutions could not be attributed to the TiO_2 phase. However, it is known that TiO_2–$Ti_3C_2T_x$ composites exhibit good H_2 evolution performance which is attributed to improved charge separation in TiO_2–$Ti_3C_2T_x$ heterojunctions [37]. Consequently, surface oxidation of MXene in alkaline solutions could contribute to increased H_2 production.

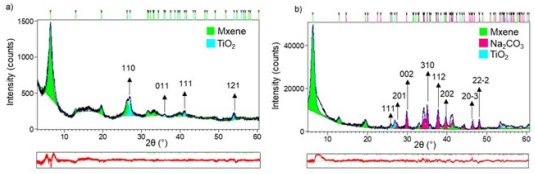

Figure 8. Rietveld refinement of dry products after the reaction in 2 M NaOH, dried at (a) 35 °C and (b) 65 °C for 10 h. Experimental diffraction data are given as black dots and calculated pattern in shown in blue. Green, cyan and magenta vertical marks represent the position of reflections of MXene, rutile and sodium carbonate, respectively. The difference curve in given below, in red.

$$H_2O + h^+ \rightarrow OH^\bullet + H^+$$

$$O_2 + e^- \rightarrow O_2^{\bullet-}$$

$$O_2^{\bullet-} + e^- + 2H^+ \rightarrow H_2O_2$$

$$O_2^{\bullet-} + H_2O \rightarrow {}^\bullet HO_2 + OH^-$$

$$OH^- + h^+ \rightarrow OH^\bullet$$

$$(- CH_2 - CH_2 -)_n + OH^- \rightarrow (- {}^\bullet CH - CH_2 -)_n + H_2O$$

$$(- {}^\bullet CH - CH_2 -)_n + O_2 \rightarrow (- CH_2 - {}^\bullet HCOO - CH_2 -)_n$$

$$(- CH_2 - {}^\bullet HCOO - CH_2 -)_n + (- CH_2 - CH_2 -)_n \rightarrow (- CH_2 - HCOOH - CH_2 -)_n + (- {}^\bullet CH - CH_2 -)_n$$

$$(- CH_2 - HCOOH - CH_2 -)_n \rightarrow (- CH_2 - {}^\bullet HCOO - CH_2 -)_n + H^+$$

$$(- CH_2 - {}^\bullet HCOO - CH_2 -)_n \rightarrow (- CH_2 - {}^\bullet HCO - CH_2 -)_n + OH^\bullet$$

$$CO_2 + e^- + H^+ \rightarrow {}^\bullet COOH$$

$$^\bullet COOH + e^- + H^+ \rightarrow CO + H_2O$$

$$^\bullet COOH + e^- + H^+ \rightarrow CO + H_2O$$

$$(-CH_2 - CH_2 -)_n \xrightarrow{^\bullet OH, O_2} 2nCO_2$$

Scheme 1. Possible reactions during photocatalytic breakdown of PE.

Finally, to understand the difference in PE degradation in aqueous solutions with and without NaOH, we characterized the production of reactive oxygen species (ROS) in these cases. It is known that the ROS production, including species produced, and consequently photocatalytic activity can be affected by the pH [46, 47]. ROS detection is critical for the understanding of the degradation process, but the free radicals have very short lifetimes due to their reactivity. Consequently, they are either studied indirectly, by using scavengers for specific ROS and investigating their effect on the photocatalytic degradation [46, 47], or directly using spin traps which react with short lived radicals to generate more long lived adducts which can then be detected using electron paramagnetic resonance spectroscopy (EPR) measurements [46, 48–51]. Spin trap molecules react with ROS produced and a combination of a spin trap and a specific ROS has a characteristic EPR spectrum which enables the identification of ROS [46, 48, 51] Due to their different sensitivity to various ROS species, different spin traps can be used to detect different ROS, or the same spin trap can be used to identify ROS produced based on the characteristic peak pattern in the EPR spectrum [46, 48, 51]. Here, we performed EPR spectroscopy using 5-(diethoxyphosphoryl)-5-methyl-1-pyrro-line-N-oxide (DEP-MPO) spin trap [48–51], which was reported to have improved stability for the detection of superoxide ion radicals [49]. Superoxide ions $O_2^{\bullet-}$ and $OH^\bullet$ radicals have been previously reported to be involved in the photocatalytic breakdown of PE [12, 29]. It was also previously proposed that photoconversion of PE and water into syngas involved reduction of water by conduction band electrons into H_2, while various radicals produced by reactions involving photogenerated holes oxidized the plastics into CO_2, and CO was produced by reduction of CO_2 [24]. The proposed reactions for the breakdown of PE are shown in scheme 1 [12, 24]. While the main reaction in the plastic degradation is oxidative cleavage of C–C bonds, there are a number of different ROS generated in the process and products of various reactions can also react among themselves. Consequently, it is expected that different

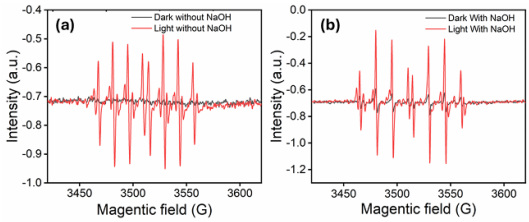

Figure 9. EPR spectra of water solutions of MXene photocatalyst with DEPMPO spin trap (a) without and (b) with 5 M NaOH.

proportions of oxidizing radical species, such as $OH^{\bullet}$, and reducing species, such as $O_2^{\bullet-}$, would result in different proportions of reaction products.

From figure 9, we can observe that without NaOH there is no signal without illumination, while with NaOH even in the dark a weak signal corresponding to DEPMPO-$OH^{\bullet}$ can be observed, confirming the reactive nature of 5 M NaOH solutions. With illumination, both with and without NaOH, we can detect both signals corresponding to DEPMPO-$OOH^{\bullet}$ and DEPMPO-$OH^{\bullet}$ [48–50]. The signals from DEPMPO-$OOH^{\bullet}$ and DEPMPO-$OH^{\bullet}$ adducts can be easily distinguished in EPR spectra by the position of the peaks, and both types of adducts are similarly long-lived, minimizing the possibility of misinterpretation of the results due to transformation between adducts [48, 49], although with prolonged time some conversion of DEPMPO-$OOH^{\bullet}$ adducts to DEPMPO-$OH^{\bullet}$ adducts occurs [50]. We observe that the signal amplitude is enhanced for 5 M NaOH, and the ratio of DEPMPO-$OOH^{\bullet}$ and DEPMPO-$OH^{\bullet}$ changes, and the signal is dominated by DEPMPO-$OH^{\bullet}$. In both cases, some additional weak peaks are observed, which could originate from DEPMPO-$H^{\cdot}$ or alkylperoxyl radicals [48, 51], but these radicals are present at much lower concentrations compared to dominant $O_2^{\bullet-}$ and $OH^{\bullet}$ radical species. It should also be noted that the initial amplitude and the duration of DEPMPO-$OOH^{\bullet}$ signal decay is pH dependent [49], but this is not expected to affect the results since the measurements are completed in a much shorter time than the half-life of the signal. Thus, EPR measurements indicate that in alkaline solution $OH^{\bullet}$ radical generation is increased, which would be expected with the abundance of OH^{-}. This is also consistent with the report of suppression of $OH^{\bullet}$ generation in acidic solutions [46]. While the ratio of DEPMPO-$OH^{\bullet}$ to DEPMPO-$OOH^{\bullet}$ is also increased, the signal intensity of DEPMPO-$OOH^{\bullet}$ is increased compared to 0 M NaOH. Thus, the enhancement of the $OH^{\bullet}$ radical production in 5 M NaOH leads to increased oxidation of PE, with an overall increased abundance of different ROS leading to the production of various gases.

In general, the photocatalytic degradation of PE in oxygen rich atmosphere proceeds along the reactions shown in scheme 1 [12, 24, 52], while in an inert atmosphere H^{+} can be reduced by conduction band electrons into H_2 [52]. However, the reaction atmosphere has not changed for 0 M and 5 M conditions. Therefore, we can conclude that there are other factors which shift the balance of redox reactions occurring at the surface so that proton reduction into H_2 becomes more favorable compared to oxygen reduction to superoxide ions [53]. It has been proposed that $OH^{\bullet}$ radicals serve as hole scavengers, and this could result in an excess of photogenerated electrons which can then participate in reduction reactions for hydrogen production [54]. It has also been shown that the photocatalytic production of hydrogen from sugars is close to zero in the absence of NaOH, while the rate of hydrogen production increased with increased concentration of NaOH, which is attributed to the increased rate of $OH^{\bullet}$ production and sugar oxidation [55]. In addition, an increased mass loss was observed for photocatalyst-PE composite films in the presence of a base, which was attributed to increased $OH^{\bullet}$ production [56]. Furthermore, isotopic experiments on H_2 production during plastic (PET, PLA, PE) degradation using CN_x/Ni_2P photocatalysts in aqueous KOH confirmed that H_2 originated from water and increased hydrogen production with increasing pH could not be entirely attributed to increased plastic solubility [30]. Thus, we can conclude that the addition of NaOH increases $OH^{\bullet}$ radical generation from the measured EPR spectra (figure 9 and literature reports [55, 56]), which increases the consumption of photogenerated holes and consequently results in an excess of photogenerated electrons. This can shift the balance of reduction reactions to proton reduction and the production of H_2 instead of oxygen reduction and the production of superoxide ions, especially at later stages of the reaction when some oxygen has been consumed in PE oxidation, consistent with the observed variations in produced gases with illumination time (figure S9). However, we cannot rule out the reactions between dissolved CO_2 and NaOH as a reason for reduced CO_2 production in alkaline solutions, and we expect that complex reactions occur due to the capability of MXene for photocatalytic degradation of various organic compounds, water splitting, and CO_2 reduction.

Finally, to examine the reusability of MXene photocatalysts, reuse under 0 M conditions was attempted, as it is obvious that MXene in alkaline 5 M NaOH solutions is not stable from the changes in FTIR (figure S16) and the fact that CH_4 gas was detected under illumination in the absence of PE. While MXene under 0 M conditions exhibit good stability for shorter time periods, as evidenced by the lack of change in FTIR spectra after 6 h for 0 M NaOH (figure S16), it is known that MXene is susceptible to oxidation under illumination. Therefore, we tested the reusability of MXene, and we can observe that the PE degradation in the second cycle is lower compared to the first, as shown in figure S18. One possible reason, in addition to the expected oxidation of MXene in aqueous solution under illumination over time, is impaired mixing of hydrophobic PE with MXene during the second cycle, as shown in figure S19. As the MXene after drying sticks to the reaction vessel, it cannot be mixed well with PE as fresh unused MXene powder.

Nevertheless, it is necessary to improve MXene stability for practical applications, in particular in alkaline media. It has been shown that surface coatings, such as atomic layer deposited (ALD) ultrathin layers, can inhibit photocorrosion and enhance reusability of different photocatalysts [57–59], including MXene containing photocatalysts [57]. Thus, further work should include the investigation of ALD-coated MXene photocatalysts, including the optimization of coating material and coating thickness in order to retain or enhance photocatalytic activity, retain pH-controlled tunability of evolved gases while improving photocatalyst stability (especially in alkaline media) and reusability.

3. Conclusion

We found that Ti_2CT_x MXene is an efficient photocatalyst for photoconversion of PE MPs (pristine and environmental). Without the addition of NaOH, complete mineralization can be achieved in 56 h, with CO_2 as the dominant reaction product. In the absence of PE and NaOH, no gases are produced. In contrast, with 5 M NaOH the production of CO_2 is completely suppressed, and the dominant reaction product is H_2, produced at a rate of 25.4 μmol $g_{cat}{}^{-1}$ h^{-1}. The involvement of MXene and water in the production of different gases under illumination in alkaline environment is confirmed by experiments without PE, which result in hydrogen production rate of 1.87 μmol $g_{cat}{}^{-1}$ h^{-1}. The reaction is expected to lead to eventual degradation of MXene over time, since CH_4 gas is also produced. Nevertheless, the possibility of tuning the composition of evolved gases by changing the solution pH is a particularly interesting aspect of MXene photocatalysts for PE degradation. Possible approaches to improve MXene oxidation stability include changing the reaction medium from water to organic solvent, lowering the temperature, or applying surface protection layers [37].

4. Experimental section

Materials: Model MPs (PE ∼5–10 μm) were procured from Henan Alfa Chemicals (Zhengzhou, China). DEPMPO (M_W = 235.22 Da, Purity > 99%) was obtained from Abcam Limited (Cambridge, UK). Ti_2CT_x MXene was synthesized according to a previously reported procedure [36]. Briefly, Ti_2AlC MAX phase powder (>99% purity, Laizhou Kai Ceramic material Co., Ltd), conductive carbon black (TIMCAL SUPER P Li™, 40 nm diameter, 62 m^2 g^{-1} surface area, TangFeng Tech. Inc.), polyvinyl alcohol (PVA, 1 wt.%), and hydrochloric acid (HCl) were used as received. The composite electrode was prepared by mixing Ti_2AlC and carbon black at a mass ratio of 95:5 with 1 ml PVA as binder. After grinding and sonicating the 10 mg mixture for 30 min, electrochemical etching was performed in a three-electrode configuration using 1 M HCl electrolyte at 0.3 V vs. RHE for 9 h at 50 °C. The etched MXene was collected from the carbon fiber cloth electrode by ethanol rinsing and brief sonication (∼20 s), then purified through multiple steps: sonication at room temperature for 30 min, centrifugation at 2,000 rpm for 15 min, supernatant collection and centrifugation at 9,000 rpm for 10 min, followed by repeated ethanol washing and sonication to remove residual MAX phase and carbon black, yielding approximately 5 mg of purified Ti_2CT_x MXene sheets.

Environmental samples: Environmental samples were extracted from a water sample collected in Tsing Lung Tau, with latitude and longitude coordinates (22.35713, 114.03479), located on the southwest coast of the New Territories in Hong Kong, following previously described procedures for sample collection and treatment [23, 42, 43]. No shape or polymer sorting was done prior to the degradation process, and the samples were ground into particles with size of ∼2 μm for degradation using ball milling (Retsch, PM400) [23]. It should be noted, however, that ball milling produces samples which are prone to aggregation, with particles sticking together. As each environmental sample after ball milling weighed in the range 11–14 mg, given the small quantity and cohesive nature of the milled material, precise mass measurement of individual aliquots was challenging. To ensure consistency in the catalyst-to-PE ratio across experiments, the entirety of

the processed sample was utilized. This approach prioritized maintaining the critical stoichiometric relationship over exact mass uniformity, thereby preserving the integrity of the experimental design.

Characterization: To characterize Ti_2CT_x samples. FTIR measurements were carried out by using Vertex 70 v (Bruker) in transmission mode. KBr was baked for 12 h under vacuum at 120 °C for further use. Ti_2CT_x 0 M NaOH was used as received. The illuminated sample (labeled as 0 M + 6 h) was obtained by placing the Ti_2CT_x under the simulated solar light (Zolix Instruments CO., LTD) for 6 h. The Ti_2CT_x with 5 M NaOH was collected with the following method. The Ti_2CT_x sample was added into 5 M NaOH solution with 6 h stirring and then washed and collected by centrifugation and dried under vacuum at 60 °C. Ti_2CT_x samples were added into KBr with a concentration of approximately 1% of the KBr (1 mg sample/100 mg KBr) and pressed into pellets. The FTIR spectra of the plastic samples and the sample:KBr powder pellets (typically 4 mg sample/500 mg KBr) were measured using an FTIR spectrometer PerkinElmer Spectrum Two.

EPR equipped with an X-band microwave (EMXPlus, Bruker) was utilized to detect hydroxyl radicals ($^{\bullet}OH$) and superoxide ions ($O_2^{\bullet-}$). The following parameters were used: frequency of 9.847 GHz, time constant of 0.16 ms and microwave power of 6.325 mW. A 5 mg sample of the liquid spin trap DEPMPO (purity > 99%) was diluted with 1 ml of deionized water. Subsequently, 400 μl of the DEPMPO solution was added to a mixture containing 20 mg of Ti_2CT_x and 5 ml of H_2O or 5 M NaOH/H_2O. The mixture was then placed in the dark and exposed to simulated solar light (Zolix Instruments CO., LTD) for 5 min. The reacted liquid DEPMPO was extracted using a capillary tube and measured. The average particle size was determined using a ZetaView nanoparticle tracking analyzer (NTA), Particle Metrix PMX 120-Z model. Microplastic particles were diluted with water and manually injected into the NTA for analysis. The resulting data provide both the particle size distribution and a corresponding Bell curve.

Morphology and the structural characterization of MXene: Ti_2CT_x sample was investigated using a scanning electron microscope (SEM, JEOL Model JSM-6490). Powder x-ray diffraction (XRD) patterns of MXene were obtained with a Rigaku smart lab 9 kW system (Rigaku, Japan), coupled to a 2D detector and utilizing Cu Kα radiation ($\lambda = 0.154$ nm).

Photocatalytic degradation of microplastics: A mixture of 50 mg of catalyst and 10 mg of microplastic was dispersed in a square cuvette containing 30 ml of deionized water. The mixture was stirred at 350 rpm using an overhead mechanical stirrer and exposed to simulated solar illumination generated by a Mullar Electronik Optik solar simulator (Xenon lamp TYP SVX 1450, with the emission spectrum shown in figure S20 and measured power density of 409 Wm^{-2}) with a horizontal beam. The plastics degradation was estimated by mass loss. Mass loss at fixed time intervals is a commonly used method to determine plastic degradation. However, separating microplastic from the solution using filter paper can introduce errors and uncertainties due to mass loss, as micro/nanoplates may adhere to filter paper. From the color of the filter and the filtered solution, it is clear that some photocatalyst remains suspended in filtered liquid, while some is mixed with MPs on the filter (see Note S1). To circumvent this issue, the initial mass of microplastic (M_0), the initial mass of photocatalyst (M_{pc}) and the mass of the square cuvette (M_{sc}) were measured. After each interval, the sample was dried in a vacuum oven at 70 °C, cooled down to room temperature, and the total mass (M_T) was measured. The mass loss of plastic (ΔM) was then calculated as $\Delta M = (M_0 + M_{pc} + M_{sc})\text{-}M_T$. The mass of the photocatalyst for 0 M NaOH remains unchanged as the photocatalyst remains stable under these conditions (there are no evolved gases from illuminated photocatalyst suspension and no observed mass loss). It should be noted that the mass loss could not be reliably measured in 5 M NaOH solutions, for several reasons: (1) change in the photocatalyst mass due to instability in alkaline solutions, (2) change in the mass of dried solid products due to various surface adsorbates on oxidized surfaces after NaOH exposure and (3) change in the mass of dried solid products since bases such as NaOH can react with dissolved CO_2 [12, 24]. The mass was measured using a Mettler Toledo XSR105 with a hanging mass pan, which ensures high stability and exceptional repeatability. The mass of environmental MP samples was measured using an analytical semi-micro balance Precisa ES 125SM, as a more precise Mettler Toledo XSR105 balance was not available at the time. To test the reusability of the photocatalyst, one cycle of degradation with measurements at 24 h intervals was completed (72 h to reach 0% residual mass). Then, fresh PE particulates (equivalent to the initial loading mass of 10 mg) were reintroduced into the reaction mixture. Subsequent degradation kinetics were evaluated at 12 h intervals during the secondary catalytic cycle.

To analyze the evolved gases, a reaction mixture containing (10 mg of catalyst and 10 mg of PE, unless specified otherwise, see table S2) was prepared in 5 ml of NaOH solution at varying concentrations (5 M, 2 M, or 0 M). After the reaction proceeded in a sealed tube (multichannel photoreactor Photosyn-10, Shanghai Quanhuan Technology Co., Ltd, with stirring and under illumination with 365–800 nm solar light at room temperature), the generated gas was collected with a 20 ml syringe and transferred to an aluminum

gas bag. The gas bag was then connected to a gas (GC) system (Agilent 8860), and the sample was manually injected into the column. Gas chromatographic analysis produced distinct peaks in both the flame ionization detector (FID, detection limit 0.1 ppm) and the thermal conductivity detector (TCD, detection limit 100 ppm). The products were identified by comparing the retention times with reference standards, and quantification was achieved by integrating the area under each peak and applying a previously established calibration curve.

Data availability statement

The data cannot be made publicly available upon publication because they are not available in a format that is sufficiently accessible or reusable by other researchers. The data that support the findings of this study are available upon reasonable request from the authors.

Acknowledgment

This work was funded by the Environment and Conservation Fund (ECF Project No. 141/2021). Any opinions, findings, conclusions or recommendations expressed in this material/event do not necessarily reflect the views of the Government of the Hong Kong Special Administrative Region and the Environment and Conservation Fund. This work is also supported by the Grant from the Research Grants Council of Hong Kong (GRF no. 15303123) and HKPDFS (ref. no. PDFS2324-5S09).

Author contributions

Atta Ur Rehman 0000-0001-8324-7305
Investigation (equal), Visualization (equal), Writing – review & editing (equal)

Sin Yi Pang
Investigation (equal), Visualization (equal), Writing – review & editing (equal)

Kang Ding Han 0009-0001-6609-0737
Investigation (supporting), Writing – review & editing (equal)

Chunyang Dong
Investigation (supporting), Writing – review & editing (equal)

Yingchuan Zhang
Investigation (supporting), Writing – review & editing (equal)

Yanling He
Investigation (supporting), Writing – review & editing (equal)

Christelle A Not 0000-0002-1386-6079
Resources (equal), Writing – review & editing (equal)

Alan Man Ching Ng
Funding acquisition (supporting), Writing – review & editing (equal)

Jianhua Hao 0000-0002-6186-5169
Funding acquisition (supporting), Writing – review & editing (equal)

Jasminka Popović
Visualization (equal), Writing – review & editing (equal)

Zheng Xiao Guo 0000-0001-5404-3215
Funding acquisition (supporting), Writing – review & editing (equal)

Aleksandra B Djurišić 0000-0002-5183-1467
Funding acquisition (lead), Writing – original draft (lead), Writing – review & editing (equal)

References

[1] Chen J, Wu J, Sherrell P C, Chen J, Wang H, Zhang W X and Yang J 2022 *Adv. Sci.* **9** 2103764
[2] Hamd W, Daher E A, Tofa T S and Dutta J 2022 *Front. Mar. Sci.* **9** 885614
[3] Kumar R 2023 *Adv. Sustain. Syst.* **7** 2300033
[4] Janani R, Bhuvana S, Geethalakshmi V, Jeyachitra R, Sathishkumar K, Balu R and Ayyamperumal R 2024 *Environ. Res.* **241** 117666

[5] Assis G C, Antonelli R, Dantas A O S and Teixeira A C S C 2023 *J. Environ. Chem. Eng.* **11** 111107
[6] Chang L and Xia Y 2024 *Small Sci.* **4** 2300096
[7] Lin J, Cheng Q, Kumar A, Zhang W, Yu Z, Hui D, Zhang C and Shang S 2025 *Trends Anal. Chem.* **183** 118082
[8] Zhao M, Zou G, Li Y, Pan B, Wang X, Zhang J, Xu L, Li C and Chen Y 2025 *Biochar* **7** 31
[9] Ariza-Tarazona M C, Villarreal-Chiu J F, Hernández-López J M, De la Rosa J R, Barbieri V, Siligardi C and Cedillo-González E I 2020 *J. Hazard. Mater.* **395** 122632
[10] Saifuddin M, Ghaffari Y, Park S Y and Kim C G 2022 *Environ. Res.* **212** 113422
[11] Ariza-Tarazona M C, Villarreal-Chiu J F, Barbieri V, Siligardi C and Cedillo- González E I 2019 *Ceram. Int.* **45** 9618–24
[12] Jiao X *et al* 2020 *Angew. Chem., Int. Ed.* **59** 15497–501
[13] Xue Z, Yu X, Ke X and Zhao J 2024 *Environ. Sci.: Nano* **11** 113–22
[14] Noor S F M, Paiman S H, Nordin A H, Ngadi N, Malek N A N N and Hamed N K A 2024 *Chem. Eng. Res. Des.* **201** 194–208
[15] Ran J, Talebian-Kiakalaieh A, Zhang S, Hashem E M, Guo M and Qiao S Z 2024 *Chem. Sci.* **15** 1611–37
[16] Paiman S H, Noor S F M, Ngadi N, Nordin A H and Abdullah N 2023 *Chem. Eng. J.* **467** 143534
[17] Kim J Y and Youn D H 2023 *Molecules* **28** 6502
[18] Liang X, Li X, Dong Q, Gao T, Cao M, Zhao K, Lichtfouse E, Patrocinio A O T and Wang C 2024 *Chem. Eng. J.* **482** 148827
[19] Wang J, Zhang C and Wang Y 2025 *ChemSusChem* **18** e202401700
[20] Jeyaraj J, Baskaralingam V, Stalin T and Muthuvel I 2023 *Environ. Res.* **233** 116366
[21] Ariza-Tarazona M C, Siligardi C, Carreón-López H A, Valdéz-Cerda J E, Pozzi P, Kaushik G, Villarreal-Chiu J F and Cedillo-González E I 2023 *Mar. Pollut. Bull.* **193** 115206
[22] Nabi I, Bacha A U, Li K, Cheng H, Wang T, Liu Y, Ajmal S, Yang Y, Feng Y and Zhang L 2020 *iScience* **23** 101326
[23] He Y, Rehman A U, Xu M, Not C A, Ng A M C and Djurišić A B 2023 *Heliyon* **9** e22562
[24] Xu J, Jiao X, Zheng K, Shao W, Zhu S, Li X, Zhu J, Pan Y, Sun Y and Xie Y 2022 *Natl Sci. Rev.* **9** nwac011
[25] Pichler C M, Bhattacharjee S, Rahaman M, Uekert T and Reisner E 2021 *ACS Catal.* **11** 9159–67
[26] Xing C, Yu G, Zhou J, Liu Q, Chen T, Liu H and Li X 2022 *Appl. Catal. B* **315** 121496
[27] Du M, Zhang Y, Wang S, Guo X, Ma Y, Xing M, Zhu Y, Chai Y and Qiu B 2022 *ACS Catal.* **12** 12823–32
[28] Nguyen T T and Edalati K 2024 *Int. J. Hydrog. Energy* **81** 411–7
[29] Mohanty C, Samal A and Das N 2024 *Int. J. Hydrog. Energy* **61** 84–93
[30] Uekert T, Kasap H and Reisner E 2019 *J. Am. Chem. Soc.* **141** 15201–10
[31] Teng J, Li W, Wei Z, Hao D, Jing L, Liu Y, Dai H, Zhu Y, Ma T and Deng J 2024 *Angew. Chem., Int. Ed.* **63** e202416039
[32] Wang L, Jiang S, Gui W, Li H, Wu J, Wang H and Yang J 2023 *Small Struct.* **4** 2300142
[33] Chu S, Zhang B, Zhao X, Soo H S, Wang F, Xiao R and Zhang H 2022 *Adv. Energy Mater.* **12** 2200435
[34] Zhang X, Jun M, Zu W, Kim M, Lee K and Lee L Y S 2024 *Small* **20** 2403347
[35] Ningsih L A, Lu P Y, Ashimura S, Yoshida M, Chen W C, Chiu Y C and Hu C 2024 *Chem. Eng. J.* **480** 148089
[36] Pang S Y, Wong Y T, Yuan S, Liu Y, Tsang M K, Yang Z, Huang H, Wong W T and Hao J 2019 *J. Am. Chem. Soc.* **141** 9610–6
[37] Murali G, Modigunta J K R, Park Y H, Lee J H, Rawal J, Lee S Y, In I and Park S J 2022 *ACS Nano* **16** 13370–429
[38] Yu S, Tang H, Zhang D, Wang S, Qiu M, Song G, Fu D, Hu B and Wang X 2022 *Sci. Total Environ.* **811** 152280
[39] Wang H, Tang Q and Wu Z 2021 *ACS Sustain. Chem. Eng.* **9** 8425–34
[40] Cao B, Wan S, Wang Y, Guo H, Ou M and Zhong Q 2022 *J. Colloid Interface Sci.* **605** 311–9
[41] Socrates G 2001 *Infrared and Raman Characteristic Group Frequencies* 3rd edn (Wiley)
[42] Ho N H E and Not C 2019 *Environ. Pollut.* **245** 702–10
[43] Masura J, Baker J E, Foster G D, Arthur C and Herring C 2015 NOAA technical memorandum NOS-OR&R; 48 (available at: https://repository.library.noaa.gov/view/noaa/10296)
[44] Ma X *et al* 2022 *ACS Appl. Nano Mater.* **5** 2848–58
[45] Pang S Y, Io W F, Wong L W, Zhao J and Hao J H 2020 *Adv. Sci.* **7** 1903680
[46] Wen Y, Wang Z, Cai Y, Song M, Qi K and Xie X 2022 *Chemosphere* **295** 133784
[47] Cao H, Lin X, Zhan H, Zhang H and Lin J 2013 *Chemosphere* **90** 1514–9
[48] Bačić G, Spasojević I, Šećerov B and Mojović M 2008 *Spectrochim. Acta A* **69** 1354–66
[49] Roubaud V, Sankarapandi S, Kuppusamy P, Tordo P and Zweier J L 1997 *Anal. Biochem.* **247** 404–11
[50] Mojović M, Vuletić M and Bačić G 2005 *Ann. New York Acad. Sci.* **1048** 471–5
[51] Karoui H, Chalier F, Finet J P and Tordo P 2011 *Org. Biomol. Chem.* **9** 2473–80
[52] Li W, Zhao W, Zhu H, Li Z J and Wang W 2023 *J. Mater. Chem. A* **11** 2503–27
[53] Zhang Y, Qi M Y, Tang Z R and Xu Y J 2023 *ACS Catal.* **13** 3575–90
[54] Zhao X, Liew M Y, Wang X, Yi X, Xia M, Wang Y, Pan W and Leung D Y C 2022 *ACS Appl. Energy Mater.* **5** 13200–11
[55] Kurenkova A Y, Markovskaya D V, Gerasimov E Y, Prosvirin I P, Cherepanova S V and Kozlova E A 2020 *Int. J. Hydrog. Energy* **45** 30165–77
[56] Lu P Y, Ningsih L A, Heksa A C, Hu C C, Chen W C and Chiu Y C 2025 *Polym. J.* **57** 575–86
[57] Lys A, Gnilitskyi I, Coy E, Jancelewicz M, Gogotsi O and Iatsunskyi I 2023 *Appl. Surf. Sci.* **640** 158336
[58] Zhao H, Deng W and Li Y 2018 *Adv. Compos. Hybrid Mater.* **1** 404–13
[59] Gao L, Nefzaoui E, Marty F, Erfan M, Bastide S, Leprince-Wang Y and Bourouina T 2021 *Catalysts* **11** 1289